Geomechanics and Engineering, *Vol. 42, No. 5 (2025) 333-345*
https://doi.org/10.12989/gae.2025.42.5.333

A disaster mitigation method for uneven ground fissure settlement deformation based on rigid isolation walls: A case study in Beijing Capital International Airport ground fissure

Huandong Mu*[1,2], Ye He[2a], Yahong Deng[1,3b] and Haiqin She[4c]

[1]*School of Geological Engineering and Geomatics, Chang'an University, South Second Ring Road, Beilin District, Xi'an 710054, People's Republic of China*
[2]*Institute of Geotechnical Engineering, Xi'an University of Technology, 5 Jinhua South Road, Xi'an 710048, People's Republic of China*
[3]*Key Laboratory of Western Mineral Resources and Geological Engineering, Ministry of Education, Chang'an University, South Second Ring Road, Beilin District, Xi'an 710054, People's Republic of China*
[4]*Baoji City Bureau of Natural Resources and Planning, Baoji 721004, 125 Baoguo Road, Administrative Center Building 1, Baoji 721004, People's Republic of China*

(*Received October 28, 2024, Revised June 23, 2025, Accepted July 30, 2025*)

Abstract. With the continuous expansion of urban construction land and the development and utilization of underground space, the conflict between ground fissures, which are widely developed in urban areas, and urban construction has become increasingly prominent. It has become a particularly prominent geological problem in urban construction, seriously affecting the planned construction of urban buildings and the safe service of the entire life cycle of existing infrastructure. Based on the principle of limit equilibrium, the calculation formulas of soil pressure, internal force and lateral displacement of the isolation wall are derived, and the variation laws of soil pressure and lateral displacement of the isolation wall under different wall parameters and soil parameters are analyzed, and the applicability of the theoretical formula was verified through numerical simulation. On this basis, taking the ground fissures site of Beijing Capital International Airport as an example, and a disaster mitigation method for Beijing Capital International Airport ground fissure settlement deformation based on rigid isolation walls was proposed. Research shows that the soil pressure of the isolation wall above the intersection point of the ground fissure and the isolation wall is distributed in a triangular pattern, and below the intersection point, it is distributed in a trapezoidal pattern, the analytical solution and the numerical solution have the same changing trend, the soil pressure at any depth obtained by the analytical solution is always greater than that of the numerical solution, which is approximately 1.11 times. With the increase of the thickness of isolation wall, the soil pressure of isolation wall gradually increases and the lateral displacement gradually decreases. When the wall thickness increases from 0.5m to 1.5m, the maximum soil pressure value increases by 5.62% and the lateral displacement at the top decreases by 8.62%, at the bottom increases by 22.7%. When the wall thickness increased from 1.5 m to 2.5 m, the maximum soil pressure decreased by 1.16%, the lateral displacement at the top increased by 4.3%, and the lateral displacement at the bottom decreased by 15%. The soil pressure and lateral displacement of the isolation wall gradually decrease with the increase of the elastic modulus and Poisson's ratio of the soil, when the elastic modulus of the soil increases by 1.2 times, the soil pressure exerted on the retaining wall decreases by 42.02%, when the Poisson's ratio of the soil increases 0.05, the soil pressure exerted on the retaining wall decreases by 29.3%. The soil pressure and lateral displacement of the isolation wall are minimally affected by the elastic modulus of the wall, only about 1%. The disaster mitigation method based on the uneven settlement deformation of ground fissures caused by isolation wall can alleviate the ground fissures disaster at Beijing International Airport, with the increase in the active dislocation amount of ground fissures, the soil pressure, lateral displacement and bending moment of the isolation wall increase. The research results will deepen the understanding of the disaster reduction mechanism of ground fissures and provide theoretical support for the design of ground fissures disaster reduction and prevention.

Keywords: Beijing capital international airport ground fissures; disaster mitigation design method; isolation wall; limit equilibrium principle; mechanical mechanism

1. Introduction

The ground fissure is a geological phenomenon where the rock and soil mass undergoes rupture due to internal and external dynamic forces, extending to the surface to form certain fissures. It is characterized by a large number, significant scale, heavy disasters, slow onset, and sustained destruction, making it one of the most severe geological hazards. Ground fissures are predominantly developed in the southwestern part of North America, eastern Asia, and northeastern Africa (Da-yu and Li 2000, Li *et al.* 2000,

*Corresponding author, Associate Professor
E-mail: mhdyhx@xaut.edu.cn
[a]Ph.D. Student
[b]Professor
[c]Staff Member

ISSN: 2005-307X (Print), 2092-6219 (Online)

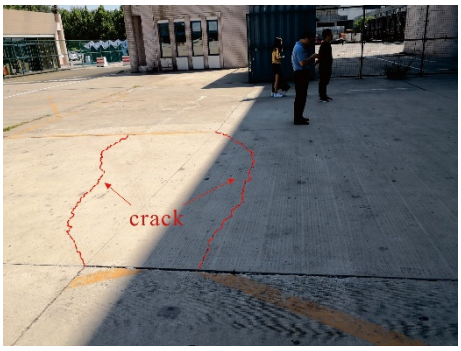

The ground of SF Express is cracked and tilted

The wall of SF Express company is cracked

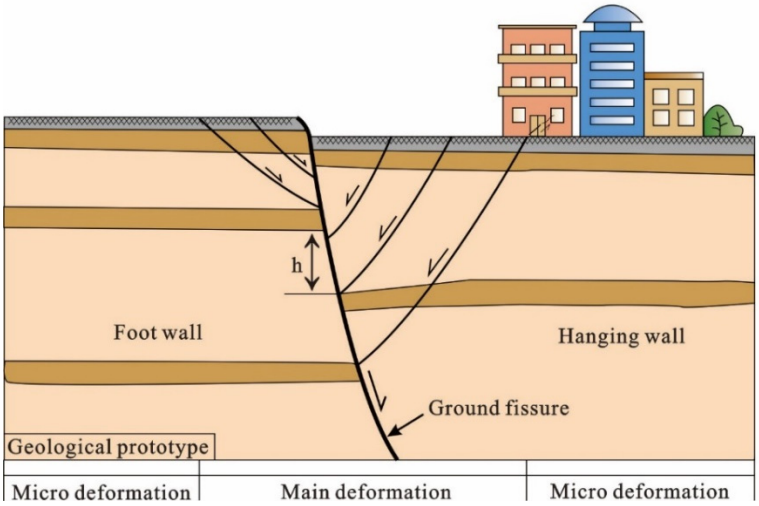

Fig. 1 Field investigation and geological prototype map of ground fissure disaster of a company

Williams *et al.* 2004, Ayalew *et al.* 2004, Pacheco *et al.* 2006, Howard and Zhou 2019). In our country, ground fissures are mainly distributed in the North China Plain, Fen-Wei Basin, and Yangtze River Delta Plain (Peng *et al.* 2018, Zhang *et al.* 2016). Among them, there are over 3,110 ground fissures developed in the North China Plain (Budhu and Muniram 2011, He *et al.* 2017, Long *et al.* 2020, Xu *et al.* 2018); over 524 ground fissures in the Fen-Wei Basin (Liu *et al.* 2018, Peng *et al.* 2020, Wang *et al.* 2018); and a staggering 25 ground fissures in the Yangtze River Delta Plain (Gong *et al.* 2020, Ye *et al.* 2018, Yun *et al.* 2008). The dense development of ground fissures has caused deformation and damage to roads and surface buildings near them (Fig. 1), posing a serious threat to the safe service life of urban infrastructure and causing huge economic losses to urban engineering construction. According to statistics, between 1950 and 2015, economic losses caused by ground fissure disasters in our country alone reached 2.4 billion yuan (Wang *et al.* 2016, Zhao *et al.* 2013). In recent years, multiple ground fissures have appeared at Beijing Capital International Airport and its surrounding areas, posing a serious threat to aviation safety (Wan *et al.* 2020). Therefore, conducting disaster reduction research on ground fissure hazards at Beijing Capital International Airport is of great theoretical significance and practical engineering application value.

Regarding ground fissure disasters, scholars have proposed a qualitative disaster reduction method to control the triggering factors of ground fissure activity, in order to prevent damage to buildings caused by ground fissures (Holzer and Pampeyan 1981).

With the deepening understanding of ground fissure hazards, the disaster reduction of ground fissures has gradually shifted from qualitative to quantitative methods. Scholars have proposed spatial avoidance as a disaster reduction method, with avoidance distances ranging from 0 to 24 meters above the ground fissure and 0 to 16 meters below it. The minimum avoidance distance needs to be determined based on the structural category and importance category of the building. This has led to the formulation of the local standard "Site Investigation and Engineering Design Code for Ground Fissures in Xi'an" (DBJ 61/T 182-2021), which is widely used in disaster reduction of ground fissures in various regions. In addition, for practical engineering purposes, some special disaster reduction methods have been applied to mitigate the hazards of ground fissure disasters, such as local dismantling, isolation, partial inundation, foundation grouting and reinforcement, and strengthening of foundation and structural strength. These disaster reduction methods to some extent can alleviate the building damage caused by the activity of ground fissures. However, it is worth noting that structural ground fissures are exposed manifestations of active faults on the Earth's surface, and their deformation is

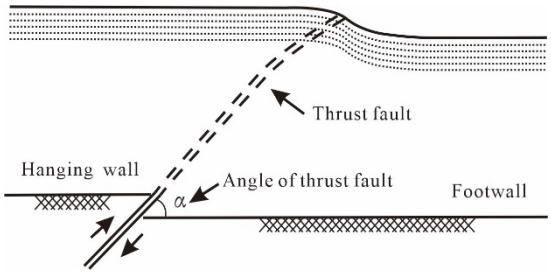

(a) Deformation map of thrust fault activity

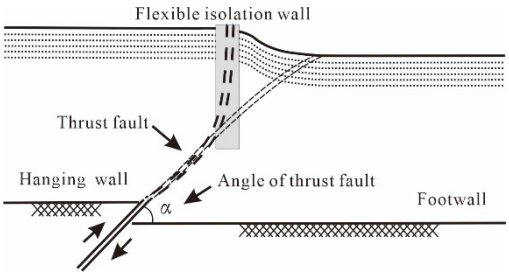

(b) Deformation map of thrust fault activity after isolation wall erection

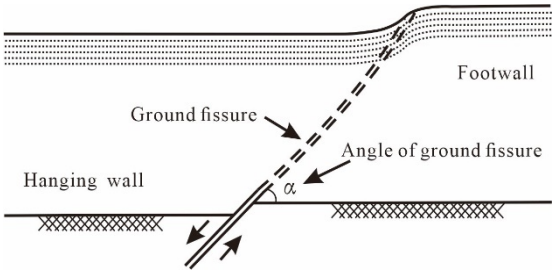

(c) Deformation map of normal fault activity

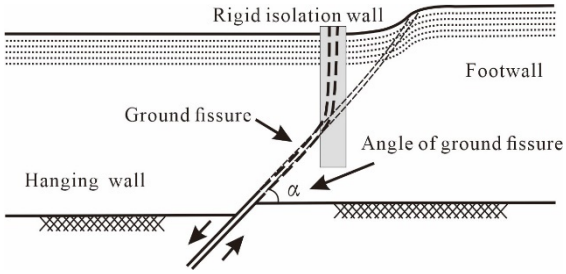

(d) Deformation map of normal fault activity after isolation wall erection

Fig. 2 Deformation maps of normal and thrust faults

clearly controlled by active faults. Therefore, disaster reduction can be achieved by changing the propagation path of active faults, drawing lessons from active faults.

The isolation wall is a protective structure for active faults, characterized by overcoming large deformations (Shahidi *et al.* 2005, Fadaee *et al.* 2013, Gazetas *et al.* 2008, Lin *et al.* 2007, Pour and Fadaee 2017). The basic principle is to use flexible isolation walls to block the rupture direction of active faults in the case of reverse faults, allowing them to extend along the wall-soil interface. The flexible isolation wall blocks the reverse thrust of the fault, protecting buildings from the propagation of ruptures caused by active faults (Figs. 2(a) and 2(b)); in the case of normal faults, rigid isolation walls are used as retaining structures to prevent buildings from being damaged by fault movements (Figs. 2(c) and 2(d)). Constructive fissures on the surface are the exposed head of normal faults, characterized by growth faulting. Therefore, disaster reduction methods based on rigid isolation walls for active faults can be applied to mitigate crack-related disasters. However, disaster reduction methods based on isolation walls for cracks are still limited to conceptual proposals and effectiveness verification. The design methods for isolation walls under the influence of cracks are not clear, greatly hindering the application of isolation walls in crack mitigation.

The ground fissure site of Beijing Capital International Airport is taken as the research object to clarify the basic characteristics of ground fissures through field investigation. A geomechanics model of the interaction between a rigid wall and the ground fissure is established using the ground fissure at Beijing Capital International Airport as a geological prototype, and calculation formulas for soil pressure, internal force, and wall deformation are derived based on the principle of limit equilibrium. The changes in soil pressure and lateral displacement of the wall with different wall and soil parameters are analyzed, and the rationality of the theoretical formula is verified by numerical simulation. Based on this, taking the ground fissures at Beijing Capital International Airport as an example, a seismic mitigation design method based on isolation walls is proposed. These research results deepen understanding of disaster reduction mechanisms related to ground fissures while providing theoretical support for disaster reduction efforts.

2. Mechanical mechanism of rigid isolation wall based on limit equilibrium principle

2.1 Numerical simulation procedure

As shown in Fig. 3, assuming mn is the ground fissure, ab is the isolation wall, point o is the intersection of the ground fissure and the isolation wall, and α is the inclination angle of the ground fissure. The soil around the isolation wall reaches the limit equilibrium state along the ground fissure. The isolation wall is divided into upper and lower parts at point o; the heights of the isolation walls in the upper and lower parts of the intersection of the ground fissure and the isolation wall are assumed to be z_1 and z_2, respectively. It is assumed that the soil in front of the isolation wall above the point of intersection with the ground fissure detaches from the wall under the action of the ground fissure, without being subjected to lateral soil pressure, while the soil at point aom behind the isolation wall is in a limit equilibrium state. The soil in front of the isolation wall below the point of intersection with the ground fissure at point boc is in a limit equilibrium state. Taking the top of the isolation wall as the origin of the coordinates, with the z -direction pointing vertically

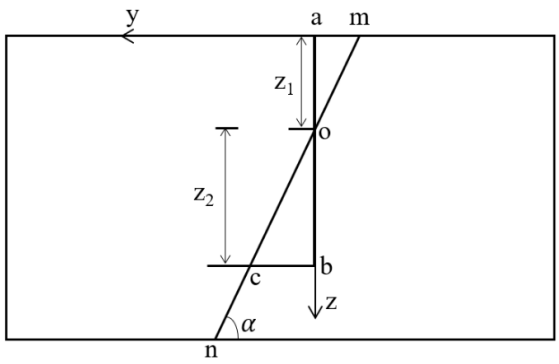

Fig. 3 Mechanical model of isolation wall

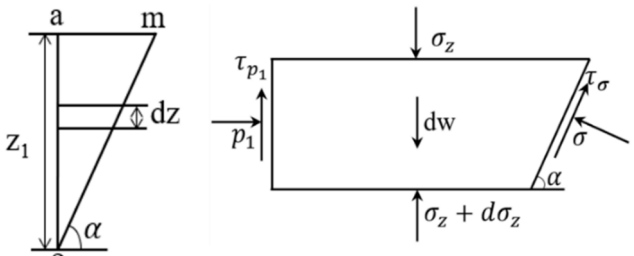

(a) (b)

Fig. 4 Stress analysis of the soil and thin layer elements of the isolation wall above the intersection of the ground fissure and the isolation wall

downward along the depth of the isolation wall, and the y-direction horizontally to the left representing the width of the soil in front of the isolation wall.

2.2 Analysis of soil pressure and internal forces of isolation walls

(1) Soil pressure behind isolation wall above the intersection of ground fissure and isolation wall

Within the range of the aom model behind the isolation wall, at a certain depth z, a thin layer element dz is arbitrarily selected as shown in Fig. 4(a), and the force analysis of the thin layer element is conducted as illustrated in Fig. 4(b). Here, dw represents the unit weight, $\sigma_z + d\sigma_z$ and σ_z are the average vertical soil pressures, γ is the gravity-weighted average value of the soil, y_r is the length of the lower boundary of the differential unit, $y_r + dz\cot\alpha$ is the length of the upper boundary of the differential unit, σ and τ_σ are the normal and shear stresses acting on the fracture surface of the upper differential unit, and p_1 and τ_{p1} represent the soil pressure and shear stress acting on the isolation wall.

When the soil behind the isolation wall is in a state of limit equilibrium, the internal friction angle of the soil is φ, the cohesion is c. The external friction angle at the wall-soil interface is φ_1, and the external cohesion is c_1. Therefore, the shear stress on the two contact surfaces is

$$\begin{aligned}\tau_{p_1} &= c_1 + p_1\tan\varphi_1\\ \tau_\sigma &= c + \sigma\tan\varphi\end{aligned} \tag{1}$$

According to the force analysis of the differential element in Fig. 4(b), the equations for static equilibrium in the horizontal and vertical directions can be respectively obtained as Eq. (2)

$$p_1 dz + \tau_\sigma\cos\alpha\frac{dz}{\sin\alpha} - \sigma\sin\alpha\frac{dz}{\sin\alpha} = 0 \tag{2}$$

$$\tau_{p_1}dz + (\sigma_z + d\sigma_z)y_r + \rho\frac{dz}{\sin\alpha} = dw + \sigma_z\omega \tag{3}$$

$$\omega = (y_r + dz\cot\alpha)$$
$$\rho = (\tau_\sigma\sin\alpha + \sigma\cos\alpha)$$

$$p_1 = k\sigma_z = k\gamma z \tag{4}$$

The simplified expression for the lateral soil pressure p_1 acting behind the isolation wall at the intersection point with the ground fissure is

$$p_1 = \frac{2\gamma z\cot\alpha}{\cot\alpha + \tan\varphi - \tan\varphi_1} + \eta \quad 0 < z < h \tag{5}$$

$$\eta = \frac{(c_1 - c)\times\lambda + c\cot\alpha(\cot\alpha + \tan\varphi)}{\lambda\times(\tan\varphi_1 - \tan\varphi - \cot\alpha)}$$
$$\lambda = 1 - \cot\alpha\tan\varphi$$

(2) Soil pressure on isolation wall under the intersection of ground fissure and isolation wall

In the boc range of the soil mass in front of the isolation wall, take a thin layer element dz at a certain depth z, and analyze the forces acting on the thin layer element, as shown in Fig. 5(b). $\sigma = \gamma z\cos\alpha$ is the normal stress perpendicular to the ground fissure, $f = \gamma z\sin\alpha$ is the frictional force along the ground fissure, γz, $\gamma(z + dz)$ are the average vertical soil pressures, $y_r - dz\cot\alpha$ is the boundary length of the differential element, σ, $f - \tau_\sigma$ represent the normal and shear stresses acting on the failure plane on the differential element, p_2, τ_{p2} represent the soil pressure and shear stress at the interface between the isolation wall and the soil mass.

Let the internal friction angle of the soil be φ, the cohesion force be c, the external friction angle of the wall-soil interface be φ_1, and the external cohesion force be c_1. When the soil in front of the isolation wall is in a state of limit equilibrium, the shear stresses τ_σ and τ_{p2} on the two contact surfaces can be expressed as

$$\begin{aligned}\tau_{p_1} &= c_1 + p_1\tan\varphi_1\\ \tau_\sigma &= c + \sigma\tan\varphi\end{aligned} \tag{6}$$

According to the stress situation of the soil mass in Fig. 5(b), the analysis of static equilibrium in the vertical direction yields

$$L\frac{dz}{\sin\alpha} + dw + N_2\gamma z = \tau_{p_2}dz + \gamma(z + dz)\gamma y_r \tag{7}$$

$$L=(f-\tau_\sigma)\sin\alpha+\sigma\cos\alpha$$

$$N_1=y_r-dz\times\cot\alpha$$

The lateral soil pressure p_2 in front of the intersection point between the ground fissure and the isolation wall is

$$p_2=\frac{1}{\tan\varphi_1}[N_2\gamma z-c_1-c] \tag{8}$$

$$N_2=(\cos\alpha\cot\alpha+\sin\alpha-\cos\alpha\tan\varphi-\cot\alpha)$$

The isolation wall behind the intersection point o of the ground fissures and isolation wall is subjected to soil pressure of p_3 and the vertical self-weight stress at a depth z in the soil behind the isolation wall is $\sigma_z=\gamma z$. Then the horizontal self-weight stress in the foundation soil is

$$\sigma_x=k_0\sigma_z \tag{9}$$

In the formula: K_0——coefficient of static soil pressure, the ratio of horizontal stress to vertical stress in a soil mass at the state of lateral confinement stress is equal to the numerical value. The value of K_0 can be determined through experimentation or calculated using empirical formulas. The following empirical formulas can be used to estimate the value of K_0.

$$K_0=1-\sin\varphi \tag{10}$$

In the formula: φ——the internal friction angle of soil.

The soil pressure p_3 acting behind the isolation wall beneath the intersection point o of ground fissures and the isolation wall is denoted is

$$p_3=(1-\sin\varphi)\gamma z \tag{11}$$

The soil pressure p_4 acting on the isolation wall beneath the intersection of the ground fissure and the isolation wall is

$$p_4=\frac{1}{\tan\varphi_1}[N_3\gamma z-c_1-c]\qquad z>h$$

$$N_3=\begin{pmatrix}\cos\alpha\cot\alpha+\sin\alpha-\cos\alpha\tan\varphi\\-\cot\alpha-(1-\sin\varphi)*\tan\varphi_1\end{pmatrix} \tag{12}$$

(3) Internal force calculation of the isolation wall

Assuming the isolation barrier is experiencing plane strain, and the angle of inclination of the ground fissure is denoted as α, the deformation differential equation representing the coordinated deformation between the isolation barrier and the soil mass is as follows

$$EI\frac{d^4x}{dz^4}-p_1(z)=0\quad 0<z<h \tag{13}$$

$$EI\frac{d^4x}{dz^4}-p_4(z)=0\quad z>h \tag{14}$$

$$\varphi=\frac{dx}{dz} \tag{15}$$

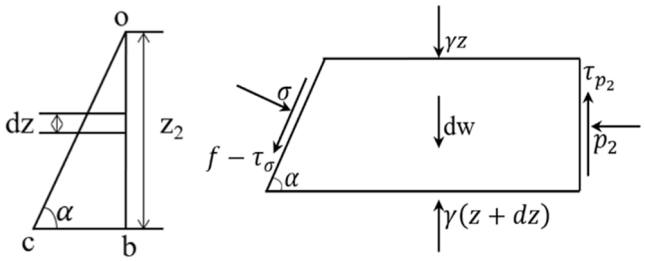

(a) (b)

Fig. 5 Stress analysis of the soil and thin layer elements of the isolation wall under the intersection of the ground fissure and the isolation wall

$$M=EI\frac{d^2x}{dz^2} \tag{16}$$

$$Q=EI\frac{d^3x}{dz^3} \tag{17}$$

In the formula: x ——the lateral horizontal displacement of the isolation wall (m); EI——the flexural stiffness of the isolation wall (kN m^2); z——depth (m); h——the intersection height of ground fissures and isolation walls (m); $p_1(z)$——the soil pressure at a depth z above the intersection of a ground fissure and a isolation wall (kPa); $p_4(z)$——the soil pressure at a depth of z below the intersection of ground fissures and isolating walls (kPa); φ——deflection of isolation wall; M——bending moment of isolation wall (kN m); Q——shear force of isolation wall (kN).

When $0<z<h$, let

$$a_1=\frac{2\gamma\cot\alpha}{\cot\alpha+\tan\varphi-\tan\varphi_1}$$

$$b_1=\frac{(c_1-c)\times(1-\cot\alpha\tan\varphi)+c\cot(\cot\alpha+\tan\varphi)}{(1-\cot\alpha\tan\varphi)\times(\tan\varphi_1-\tan\varphi-\cot\alpha)}$$

From formula (5)

$$p_1(z)=a_1z+b_1 \tag{18}$$

Substituting Eq. (18) into Eqs. (14)-(16) and (17), we can obtain the internal force Q_1 in the isolation wall

$$Q_1=\frac{a_1}{2}z^2+b_1z+c_1 \tag{19}$$

When $z>h$, let

$$a_2=\frac{\gamma}{\tan\varphi_1}(U-I)$$

$$U=(\cos\alpha(\cot\alpha-\tan\varphi)+\sin\alpha-\cot\alpha)$$

$$I=(\sin\varphi-1)\tan\varphi_1$$

$$b_2=-\frac{c_1+c}{\tan\varphi_1}$$

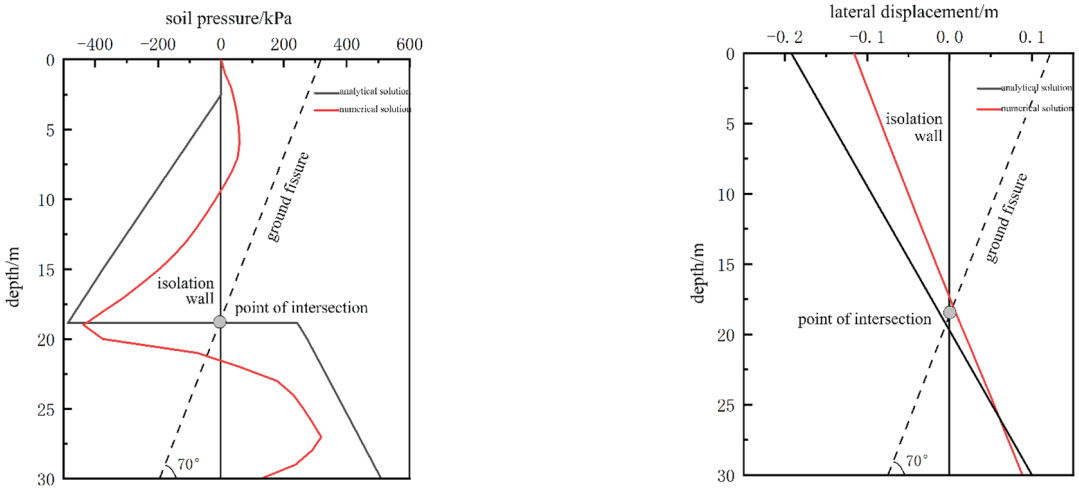

Fig. 6 Variation of soil pressure and lateral displacement of the isolation wall obtained by numerical and analytical solutions

From formula (12)

$$p_4(z) = a_2 z + b_2 \tag{20}$$

Substituting Eq. (20) into Eqs. (14)-(16) and (17), we can obtain the internal force Q_2 in the isolation wall

$$Q_2 = \frac{a_2}{2} z^2 + b_2 z + c_1 \tag{21}$$

2.3 The theory extends to verification and parameter sensitivity analysis

2.3.1 Verification of theoretical derivation

Using the example of the ground fissures at Beijing Capital International Airport, the applicability of the calculation formulas for the soil pressure and lateral displacement of the isolation wall is validated. Through alculation, the variation patterns of the soil pressure and lateral displacement of the isolation wall can be obtained as shown in Fig. 6.

The analysis of Fig. 6 shows that the trend of the change in soil pressure on the isolation wall obtained from theoretical calculations is generally similar to that obtained from numerical solutions, with the analytical solution always yielding higher soil pressure values at any depth compared to the numerical solution. The soil pressure on the isolation wall derived from the numerical solution exhibits a nonlinear distribution, with the maximum soil pressure value being 437.14 kPa. Conversely, the analytical solution shows a linear distribution of soil pressure on the isolation wall under the same conditions, with the maximum soil pressure reaching 487.28 kPa, approximately 1.11 times that of the numerical solution. It is evident that the numerical solution reasonably captures the deformation properties of the actual soil to some extent, demonstrating the continuity of soil pressure changes.

2.3.2 Sensitivity analysis of soil pressure and lateral displacement parameters of isolation walls

(1) The thickness of the isolation wall

Draw the curve of the change law of soil pressure and lateral displacement of isolation wall under different wall thicknesses as shown in Fig. 7.

From Fig. 7, it can be observed that when the wall thickness of the isolation wall increases from 0.5 m to 2.5 m, the soil pressure on the wall shows a pattern of initially increasing and then decreasing. The lateral displacement of the top of the isolation wall decreases initially and then increases with the increase in wall thickness, while the lateral displacement of the bottom increases initially and then decreases with the increase in wall thickness. When the wall thickness increased from 0.5 m to 1.5 m, the maximum soil pressure value increased by 5.62%, the lateral displacement at the top decreased by 8.62%, and the lateral displacement at the bottom increased by 22.7%; When the wall thickness increased from 1.5 m to 2.5 m, the maximum soil pressure decreased by 1.16%, the lateral displacement at the top increased by 4.3%, and the lateral displacement at the bottom decreased by 15%. It can be seen that the thickness of the isolation wall has a relatively small impact on the soil pressure and lateral displacement of the wall body.

(2) Elastic modulus of the isolation wall

The elastic modulus of the isolation wall was taken as 0.8 times, 0.9 times, 1.0 times, 1.1 times, and 1.2 times of the prototype, and the variation curves of the soil pressure and lateral displacement of the isolation wall under different wall elastic moduli are shown in Fig. 8.

According to Fig. 8, as the wall elastic modulus of the isolation wall gradually increases, the soil pressure of the wall first increases and then basically remains unchanged. The lateral displacements at the top and bottom of the wall both slowly decrease and the reduction is minimal. It can be seen that the thickness of the isolation wall has a minimal overall impact on the effectiveness of the isolation wall.

(3) The elastic modulus of the soil on both sides of the isolation wall

The elastic modulus of the soil was simulated at 0.8 times, 0.9 times, 1.0 times, 1.1 times, and 1.2 times of the original model, obtaining the variation curves of the soil pressure and lateral displacement of the isolation wall at

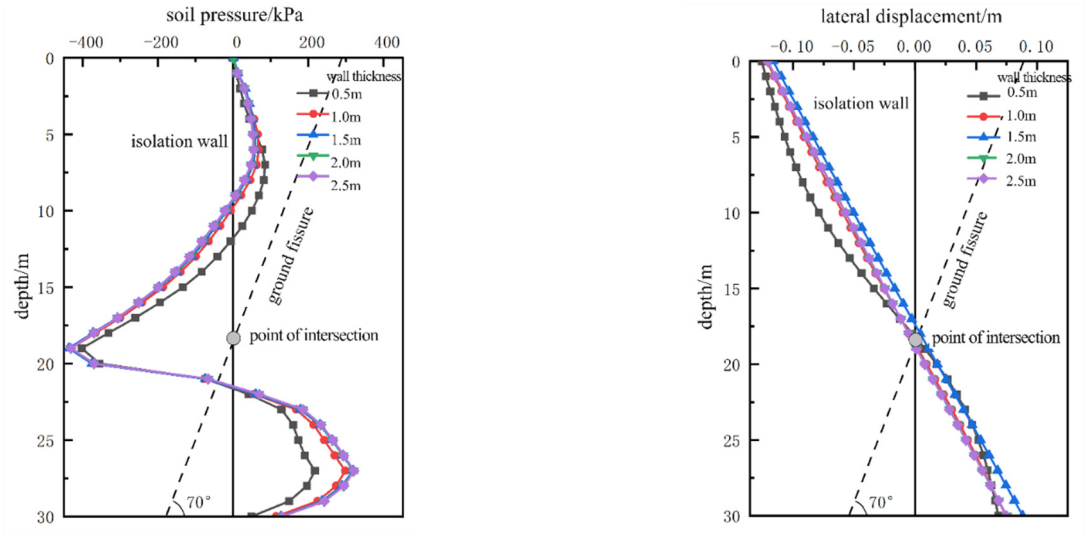

Fig. 7 Variation of wall soil pressure and lateral displacement with diverse thicknesses of isolation wall

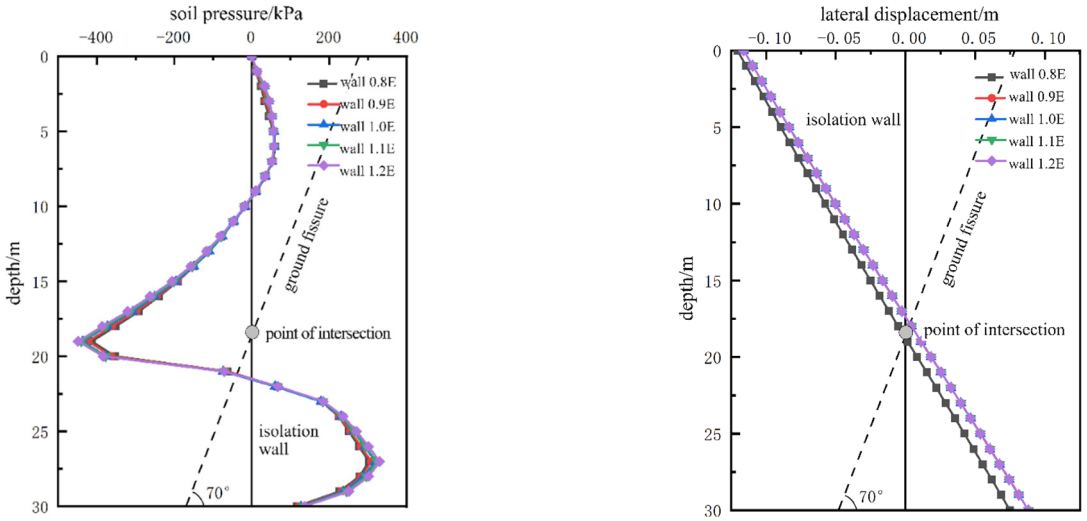

Fig. 8 Variation of wall soil pressure and lateral displacement with different elastic modulus

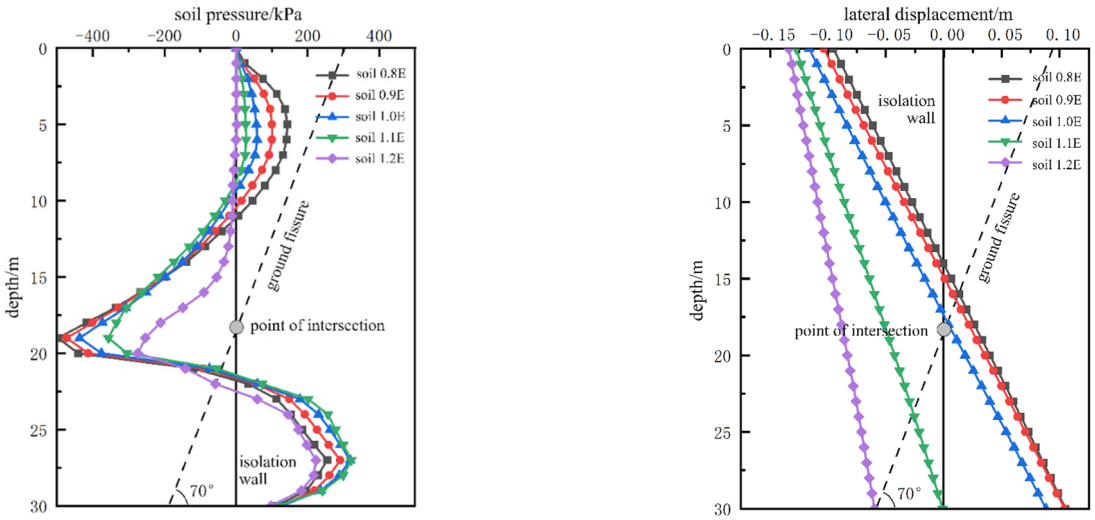

Fig. 9 Variation of wall soil pressure and lateral displacement with different soil elastic modulus

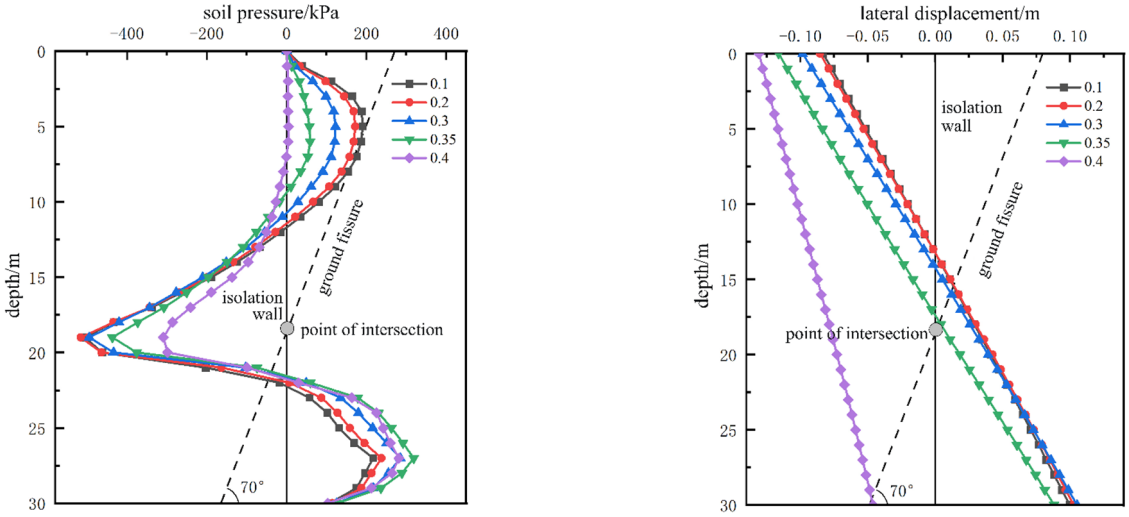

Fig. 10 Variation of wall soil pressure and lateral displacement with different Poisson's ratio of soil

different elastic moduli of the soil, as shown in Fig. 9. It can be observed from Fig. 9 that as the elastic modulus of the soil gradually decreases from 1.0 times of the original model, the maximum soil pressure acting on the isolation wall increases, the lateral displacement at the bottom of the isolation wall increases, and the lateral displacement at the top decreases. As the elastic modulus of the soil gradually increases from 1.0 times the original model, the maximum soil pressure on the isolation wall decreases, the lateral displacement at the bottom decreases, and the lateral displacement at the top increases. It can be seen that the elastic modulus of the soil has a significant impact on the soil pressure and lateral displacement of isolation wall.

(4) Poisson's ratio of the soil on both sides of the isolation wall

The Poisson's ratios of the soil were 0.1, 0.2, 0.3, 0.4, and the original Poisson's ratio of the soil was 0.35. The variation curves of the soil pressure and lateral displacement of the isolation wall with different soil elastic moduli are shown in Fig. 10.

From Fig. 10, it can be seen that as the Poisson's ratio of the original model soil gradually decreases, the maximum soil pressure on the isolation wall gradually increases, the lateral displacement at the top decreases, and the lateral displacement at the bottom increases. When the initial model's soil Poisson's ratio gradually increases, the maximum soil pressure acting on the retaining wall decreases gradually, the lateral displacement at the top increases, and the lateral displacement at the bottom decreases. It can be seen that the Poisson's ratio of the soil has a significant impact on the soil pressure and lateral displacement of the isolation wall.

3. Case analysis of disaster reduction for uneven settlement deformation of ground fissures based on isolation walls

3.1 Background of ground fissure geological environment at Beijing International Airport

Beijing is located in the northern part of the North China Plain (Fig. 11(a)), where the geological structure is complex, with the development of the NE-trending Huangzhuang-Gaoliying fault, Shunyi-Liangxiang-Qianmen fault, Nanyuan-Tongxian fault, and Xiadian fault, as well as the NW-trending Yongding River fault and Nankou-Sunhe fault (Fig. 11(b)). Due to the influence of active faults, the region is characterized by widespread development of ground fissures, particularly concentrated in the areas of Beixiaoying, Shunyi urban area, and Huangzhuang-Gaoliying (Wan *et al.* 2020). Among these faults, the Shunyi-Liangxiang-Qianmen fault zone crosses the Beijing Capital International Airport, trending NE at 25° to 35°, dipping northwest with an inclination angle of approximately 60° to 80°, classified as a positive oblique slip fault (Gao *et al.* 2019a, Wan *et al.* 2020, Zhou *et al.* 2022).

In recent years, ground fissures have developed widely in the areas around Beijing Capital International Airport, and the most obvious ones are near SF Express (Beijing Headquarters) in the north of the airport and Wuyuan Logistics in the southwest of the airport (Fig. 11(c)). The development of these ground fissures is controlled by the Shunyi-Liangxiang-Qianmen fault and is a typical structural ground fissure. In addition to being influenced by the activity of the fault zone itself, the extraction of groundwater in the area exacerbates the activity of the ground fissures. Since 2011, internal cracks have appeared at Beijing Capital International Airport, particularly noticeable in the damage to infrastructure such as Terminals 2 and 3, taxiways, runways, and adjacent areas due to varying degrees of cracking (Table 1).

According to on-site investigations, the cracks at Beijing International Airport generally develop along the NE30°~55° direction with a width of approximately 3.0~4.0 meters and a length of up to 600 meters. The cracks have resulted in different levels of damage, including the taxiways and covers on the south side of Terminal 2, the sewers and manhole covers on the southeast side, underground passages beneath runways on the east side,

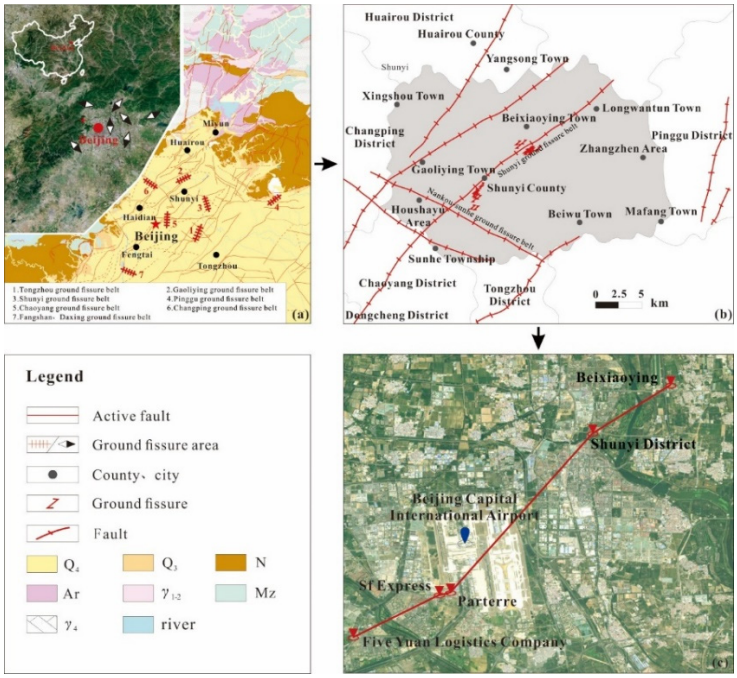

Fig. 11 Distribution maps of ground fissure in Shunyi District and Beijing Capital International Airport

Table 1 Investigation of ground fissure disaster at Beijing Capital International Airport

Location	Taxiway and covers on the south side of Terminal 2	The sewer and manhole covers on the southeast side of Terminal 2	The underground passage on the east side of the T2 terminal runway	The flowerbed on the southwest side of Terminal 2	Taxiway on the northwest side of Terminal 3 and the surrounding grassy area
Length extension /m	430	—	38	200	—
Width /cm	1~10	2~5	1~3	—	—
Bandwidth impact /m	100	50	—	20	—
Towards /°	NE55°	NE53°	NE58°	NE56°	NE60°
Tendency /°	Southeast	Southeast	Southeast	Southeast	Southeast
Dip angle /°	Subvertical	60°~70°	—	50°	70°~75°
Vertical displacement /cm	12~30	11	—	30	20
The characteristics of ground fissures.	Undulate, spread	Echelon	There is underground water seeping along the fissures.	Shear fracture	Shear fracture

and flower beds on the southwest side. In Terminal 3, there are evident steep slopes appearing in the turf area on the northwest side of the taxiing zone, with cracking on the taxiway severely affecting normal aircraft takeoff operations.

3.2 Establishment of numerical model

Taking the ground fissure site of Beijing Capital International Airport as a geological prototype, a two-dimensional plane strain model is established based on MIDAS GTS NX numerical software. The geometric size of the model is 220 m (length) ×60 m (height). The isolation wall is located on the upper side of the ground fissure, with a distance of 6.8 m from the top of the ground fissure, a height of 30 m, a width of 1.5 m, and a dip angle of 70°. At the boundary of the model, a grid unit is set every 4 m, while for the ground fissure and isolation wall positions, a grid unit is set every 1m. The numerical calculation model with grid division using a linear gradient is shown in Fig. 12.

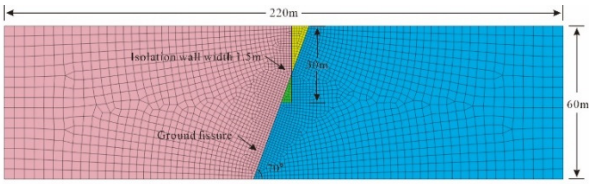

Fig. 12 Numerical simulation model of ground fissure mitigation design based on the isolation wall

The material of the site soil is assumed to be an isotropic ideal elastoplastic material that satisfies the Mohr-Coulomb strength criterion. The isolation wall is made of reinforced concrete as a rigid material, assumed to be the material parameters of an elastic beam element in the numerical simulation as shown in Table 2.

Table 2 Material parameters of the numerical model

Structural parameter	Soil compaction $\gamma/(kN/m_3)$	Elasticity modulus E/Mpa	Poisson's ratio μ	Cohesion c/kpa	Internal friction angle φ/(°)
Soil layer	17.5	8.5	0.35	40	20
Isolation wall	23.5	30000	0.2	600	35
Ground fissure	$K_n = K_t = 6.75 \times 10^4 kPa \ \ c = 10kPa \ \ \varphi = 12°$				

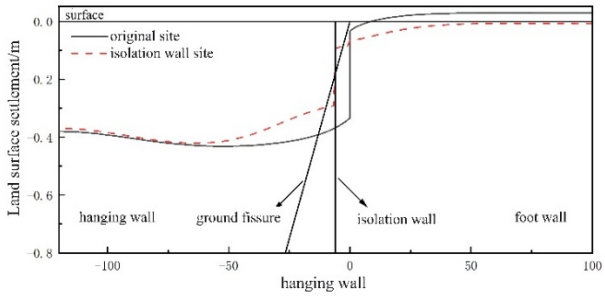

Fig. 13 The vertical displacement curve of the site surface with or without the isolation wall

The ground fissure's mode of activity involves the fixed footwall and the sliding of the hanging wall along the inclined fracture surface of the ground fissure. During loading, a forced displacement load is applied to the bottom of the hanging wall, while the footwall is subject to fixed constraints and boundary conditions. For numerical calculations, node boundary conditions are used to constrain the calculation model, ensuring convergence of the model boundaries through the imposition of static fixed constraints. Firstly, by constraining the displacement in the X-direction of the model, the semi-infinite space nature of the soil in actual conditions is simulated. Secondly, by constraining the displacement at the bottom in the Y-direction of the model, the relative stability of deep soil layers in actual conditions is simulated. Finally, static load is applied to the model to simulate the deformation of soil layers in the fissure site under the influence of self-weight stress. In numerical calculations, considering that the maximum vertical displacement of ground fissures in the next 100 years is 50 cm, five different scenarios with displacements set at 0.1 m, 0.2 m, 0.3 m, 0.4 m, and 0.5 m are analyzed.

3.3 Results and discussion

3.3.1 Comparative analysis of soil settlement deformation in ground fissure sites under the action of isolation walls

By calculating the vertical displacement of the soil mass in the absence of isolated wall ground fissure and with isolated wall ground fissures at different levels of active dislocation in various ground fissures and plotting the variation curve of the vertical displacement of the soil mass as shown in Fig. 13.

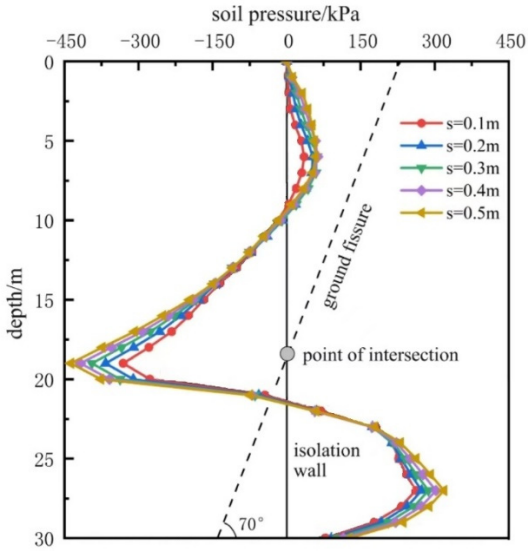

Fig. 14 Variation curve of the soil pressure on isolation wall with different ground fissure dislocations

As shown in Fig. 13, it can be seen that the vertical displacement of the surface soil layer near the front edge of the isolation wall in the area without an isolation wall is relatively large, whereas in the area with the isolation wall the vertical displacement of the ground surface is greatly reduced due to the isolating effect of the wall. The wedge-shaped soil between the isolation wall and ground fissures in the isolation wall site, as part of the upper strata, experiences minimal vertical displacement on the surface, which is greatly reduced by the action of the isolation wall. The lower strata near the ground fissures in the no isolation wall site exhibit certain vertical displacements on the surface. However, the isolation wall redirects the ground fissure activity, maintaining stability in the lower strata and preventing settlement deformation.

3.3.2 Soil pressure of the isolation wall under the action of ground fissure activities

The variation curve of the soil pressure on the isolation wall under different amounts of displacement along ground fissures is shown in Fig. 14. It can be observed from the graph that the maximum soil pressure on the isolation wall increases with the total displacement of ground fissures, with the maximum soil pressure located at the intersection of the isolation wall and the ground fissures.

Above the juncture of the isolation wall and the ground fissures, the soil pressure increases with depth. Below the juncture of the isolation wall and the ground fissures, the soil pressure on the isolation wall initially increases before decreasing, due to the vertical constraint applied at the bottom of the isolation wall, which reduces the soil pressure on the wall.

3.3.3 Lateral displacement of the isolation wall under the action of ground fissure activities

The variation of lateral displacement of isolation walls under different levels of activity dislocation of various ground fissures is shown in Fig. 15.

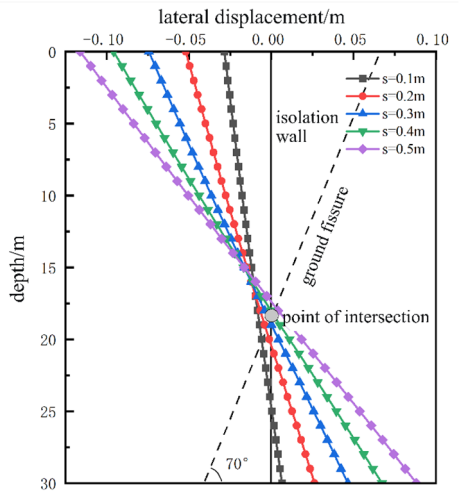

Fig. 15 Variation of the Lateral displacement with different ground fissure dislocations

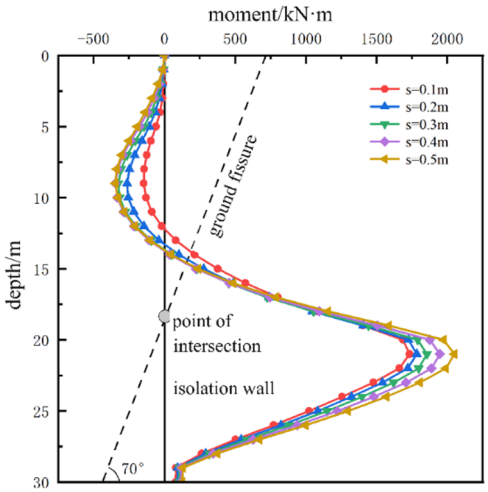

Fig. 16 Variation of the moment on isolation wall with different ground fissure dislocations

As observed from the graph, the lateral displacements at the top and bottom of the isolation wall increase with the increase in the level of activity dislocation of ground fissures, both moving away from the direction of the isolation wall. At the top of the isolation wall, the lateral displacement is caused by the lack of horizontal support from the overlying soil mass above the intersection of the isolation wall and ground fissure due to the wedge-shaped soil mass acting from the ground fissure, along with the influence of the self-weight stress of the soil mass and the lateral soil pressure from the underlying soil layer. The bottom lateral displacement of the isolation wall is due to the compression of the underlying soil mass below the intersection of the isolation wall and ground fissure caused by the impact of the ground fissure.

3.3.4 The bending moment of the isolation wall under the action of ground fissure activities

The variation curve of bending moments of isolation walls under different levels of tectonic displacement in various ground fissures is shown in Fig. 16.

Fig. 17 A thought diagram of a disaster mitigation method for uneven ground fissure settlement deformation based on rigid isolation walls

It can be observed from the graph that the bending moment of the isolation wall increases with the increase of tectonic displacement in the ground fissures. The change pattern is basically consistent with the variation pattern of the soil pressure acting on the isolation wall. The maximum bending moment occurs at the intersection of the isolation wall and the ground fissure, amounting to 2049.4 $kN \cdot m$.

4. Disaster reduction method for uneven settlement deformation of ground fissures based on isolation walls

In order to deepen the understanding of the disaster reduction mechanism of ground fissures and provide theoretical support for the design of ground fissures disaster reduction and prevention, this paper mainly takes the ground fissures at Beijing Capital International Airport as the research object. The core content is to provide the design basis of the main parameters of the isolation wall in the "Disaster reduction method of uneven settlement Deformation of ground fissures based on Isolation Wall". And provide the design ideas of the isolation wall that can be referred to for actual construction projects (as shown in Fig. 17).

Firstly, conduct on-site investigations of ground fissures and settlement areas through geological surveys to obtain data such as geological environment characteristics and spatial distribution, and construct a model of ground fissures site settlement areas. Secondly, based on this geological model and in combination with the actual disaster reduction needs, the applicability of the isolation wall technology is evaluated. If the assessment determines that it is not applicable, then turn to alternative disaster reduction plans; If applicable, it enters the design stage.

Then, based on the mechanical characteristics of soil settlement in the ground fissure site, determine the structural type of the isolation wall (such as rigid/flexible), and at the same time carry out the design of the key parameters of the isolation wall, mainly including: the depth at which the isolation wall is embedded in the soil, the horizontal distance between the isolation wall and the exposed ground fissure, and the material properties of the isolation wall, etc. Subsequently, through the dual verification of physical model tests and numerical calculations, it is determined whether the strength parameters of the isolation wall meet the requirements for resisting deformation. If the standard is not met, it will return to the parameter optimization stage; if it is met, it will enter the final evaluation.

Finally, on the basis of the compliance plan, the disaster reduction effectiveness is comprehensively evaluated from the two dimensions of deformation control and mechanical response. If the assessment is feasible, put it into practice; If there are any defects, it will be returned to the design stage for iterative optimization to form a closed-loop decision-making process, thereby ensuring the realization of the " A disaster mitigation method for uneven ground fissure settlement deformation based on rigid isolation walls".

5. Conclusions

• The calculation formulas for soil pressure and lateral displacement of the isolation wall, based on the limit equilibrium principle, are established through theoretical derivation. The soil pressure distribution above the intersection point between the ground fissure and the isolation wall is triangular, while below it is trapezoidal. The direction of the soil pressure at the intersection point changes.

• As the thickness of the isolation wall increases, the soil pressure gradually rises while the lateral displacement decreases. When the wall thickness reaches 1.5m, the changes in soil pressure and lateral displacement stabilize. The soil pressure and lateral displacement of the isolation wall decrease as the elastic modulus of the soil and Poisson's ratio increase, with little influence from the elastic modulus of the wall. Both analytical and numerical solutions exhibit similar trends and closely aligned values. The installation of an isolation wall can significantly reduce settlement deformation in the soil layer at the bottom of ground fissures, while soil pressure, lateral displacement, and bending moment of the isolation wall increase with an increase in active dislocation within ground fissures.

• The numerical simulation results indicate that vertical displacement, soil pressure, lateral displacement, and bending moment of the soil surface at Beijing International Airport increase with an increase in active ground fissure dislocation.

Acknowledgments

The research described in this paper was financially supported by the National Natural Science Foundation of China (No. 42372336) and the Chang'an University, Supported by the Special Fund for Basic Scientific Research of Central Universities (300102262505).

References

Ayalew, L., Yamagishi, H. and Reik, G. (2004), “Ground cracks in Ethiopian Rift Valley: facts and uncertainties”, *Eng. Geol*., **75**, 309-324. https://doi.org/10.1016/j.enggeo.2004.06.018.

Budhu, M. (2011), “Earth fissure formation from the mechanics of groundwater pumping”, *Int. J. Geomech*., **11**(1), 1-11. https://doi.org/10.1061/(ASCE)GM.1943-5622.0000060.

Da-yu, G. and Li, Z. (2000), “Ground fissure hazards in USA and China”, *Acta Seismologica Sinica*, **13**, 466-476. https://doi.org/10.1007/s11589-000-0029-4.

Fadaee, M., Anastasopoulos, I., Gazetas, G., Jafari, M.K. and Kamalian, M. (2013), “Soil bentonite wall protects foundation from thrust faulting: Analyses and experiment”, *Earthq. Eng. Eng. Vib.*, **12**, 473-486. https://doi.org/10.1007/s11803-013-0187-8.

Gao, M., Gong, H., Li, X., Chen, B., Zhou, C., Shi, M., Guo, L., Chen, Z., Ni, Z. and Duan, G. (2019), “Land subsidence and ground fissures in Beijing apital International Airport (BCIA): evidence from quasi-PS InSAR znalysis”, *Remote Sens.*, **11**, 1466. https://doi.org/10.3390/rs11121466.

Gazetas, G., Pecker, A., Faccioli, E., Paolucci, R. and Anastasopoulos, I. (2008), “Preliminary design recommendations for dip-slip fault-foundation interaction”, *Bull. Earthq. Eng.*, **6**, 677-687. https://doi.org/10.1007/s10518-008-9082-5

Gong, X., Geng, J., Sun, Q., Gu, J. and Zhang, W. (2020),. “Experimental study on pumping-induced land subsidence and earth fissures: a case study in the Su-Xi-Chang region, China”, *Bull. Eng. Geol. Environ.*, **79**, 1-11. https://doi.org/10.1007/s10064-020-01864-1.

He, Z., Ma, B., Long, J., Zhang, H., Liang, K. and Jiang, D. (2017), “Recent ground fissures in the Hetao basin, Inner Mongolia, China”, *Geomorphology*, **295**: 102-114. https://doi.org/10.1016/j.geomorph.2017.07.008.

Holzer, T.L. and Pampeyan, E.H. (1981), “Earth fissures and localized differential subsidence”, *Water Resour. Res.*, **17**(1), 223-227. https://doi.org/10.1029/WR017i001p00223.

Howard, K.W.F. and Zhou, W. (2019), “Overview of ground fissure research in China”, *Environ. Earth Sci.*, **78**, 97. https://doi.org/10.1007/s12665-019-8114-6.

Li, Y., Yang, J. and Hu, X. (2000), “Origin of ground fissures in the Shanxi Graben System, Northern China”, *Eng. Geol.*, **55**, 267-275. https://doi.org/10.1016/S0013-7952(99)00082-4.

Lin, M.L., Chung, C.F., Jeng, F.S. and Yao, T.C. (2007), “The deformation of overburden soil induced by thrust faulting and its impact on underground tunnels”, *Eng. Geol.*, **92**(3-4), 110-132. https://doi.org/10.1016/j.enggeo.2007.03.008.

Liu, N., Huang, Q., Wang, L., Fan, W., Jiang, Z. and Peng, J. (2018). “Dynamic characteristics research of a ground fissure site at Xi’an, China”, *Tunn. Undergr. Sp. Tech.*, **82**, 182-190. https://doi.org/10.1016/j.tust.2018.08.044.

Long, Z., Yong, L., Yumei, L., Fang, T., He, L., Kunchao, L., Te, S., Xiangru, K. and Menghan, L. (2020), “Different disaster characteristics of earth fissures and their influence factors in the Beijing plain”, *Proceedings of the International Association of Hydrological Sciences*. https://doi.org/10.5194/piahs-382-629-2020.

Pacheco, J., Arzate, J., Rojas, E., Arroyo, M., Yutsis, V. and Ochoa, G. (2006), “Delimitation of ground failure zones due to land subsidence using gravity data and finite element modeling in the Querétaro valley, México”, *Eng. Geol.*, **84**(3-4), 143-160. https://doi.org/10.1016/j.enggeo.2005.12.003.

Peng, J., Qiao, J., Sun, X., Lu, Q., Zheng, J., Meng, Z., Xu, J.,

Wang, F. and Zhao, J. (2020), "Distribution and generative mechanisms of ground fissures in China", *J. Asian Earth Sci.*, **191**, 104218-104218. https://doi.org/10.1016/j.enggeo.2005.12.003.

Peng, J., Qu, W., Ren, J., Zhang, Q. and Wang, F. (2018), "Geological factors for the formation of Xi'an ground fractures", *J. Earth Sci.*, **29**, 468-478. https://doi.org/10.1007/s12583-018-0841-1.

Pour, F.F. and Fadaee, M. (2017), "Investigating the effect of using soil bentonite wall on damage mitigation of steel buried pipelines subjected to reverse fault rupture", *Proceedings of the 6th International Conference on Computational Methods in Structural Dynamics and Earthquake Engineering Methods in Structural*, 3647-3658. https://doi.org/10.7712/120117.5672.18146.

Shahidi, A.R. and Vafaeian, M. (2005), "Analysis of longitudinal profile of the tunnels in the active faulted zone and designing the flexible lining (for Koohrang-III tunnel)", *Tunn. Undergr. Sp. Tech.*, **20**(3), 213-221. https://doi.org/10.1016/j.tust.2004.08.003.

Wan, J., Li, C. Tan, C., Feng, C., Zhang, P. and Qi, B. (2020), "Characteristics and main causes of earth fissures in northeastern Beijing Plain, China", *Bull. Eng. Geol. Environ.*, 1-17. https://doi.org/10.1007/s10064-020-01731-z.

Wang, G., You, G., Zhu, J., Yu, J. and Li, W. (2016), "Earth fissures in Su–Xi–Chang region, Jiangsu, China", *Surveys in Geophysics*, **37**, 1095-1116. https://doi.org/10.1007/s10712-016-9388-9.

Wang, Z.F., Cheng, W.C. and Wang, Y.Q. (2018), "Investigation into geohazards during urbanization process of Xi'an, China", *Nat. Hazards,* **92**, 1937-1953. https://doi.org/10.1007/s11069-018-3280-5.

Williams, F.M., Williams, M.A.J. and Aumento, F. (2004), "Tensional fissures and crustal extension rates in the northern part of the Main Ethiopian Rift", *J. African Earth Sci.*, **38**(2), 183-197. https://doi.org/10.1016/j.jafrearsci.2003.10.007.

Xu, J., Peng, J., An, H., Wang, F., Sun, H., Hu, H. and Yang, B. (2018), "Paleochannel-controlled earth fissures in Daming, North China Plain and their implication for underground paleogeomorphology", *Geomorphology,* **327**, 523-532. https://doi.org/10.1016/j.geomorph.2018.11.020.

Ye, S., Franceschini, A., Zhang, Y., Janna, C., Gong, X., Yu, J. and Teatini, P. (2018, "A novel approach to model earth fissure caused by extensive aquifer exploitation and its aApplication to the Wuxi Case, China", *Water Resour. Res.*, **54**, 2249-2269. https://doi.org/10.1002/2017WR021872.

Zhang, Y., Wang, Z., Xue, Y., Wu, J. and Yu, J. (2016), "Mechanisms for earth fissure formation due to groundwater extraction in the Su-Xi-Chang area, China", *Bull. Eng. Geol. Environ.*, **75**, 745-760. https://doi.org/10.1007/s10064-015-0775-0.

Zhang, Y., Xue, Y.Q., Wu, J.C., Yu, J., Wei, Z.X. and Li, Q.F. (2008), "Land subsidence and earth fissures due to groundwater withdrawal in the Southern Yangtse Delta, China", *Environ. Geol.*, **55**, 751-762. https://doi.org/10.1007/s00254-007-1028-8.

Zhao, H., Ma, F., Zhang, Y. and Guo, J. (2013), "Monitoring and mechanisms of ground deformation and ground fissures induced by cut-and-fill mining in the Jinchuan Mine 2, China", *Environ. Earth Sci*., **68**, 1903-1911. https://doi.org/10.1007/s12665-012-1877-7.

Zhou, Z., Yao, X., Ren, K. and Liu, H. (2022), "Formation mechanism of ground fissure at Beijing Capital International Airport revealed by high-resolution InSAR and numerical modelling", *Eng. Geol.*, **306**. https://doi.org/10.1016/j.enggeo.2022.106775.